Monthly Notices
of the
ROYAL ASTRONOMICAL SOCIETY

MNRAS **495,** 3935–3942 (2020)
Advance Access publication 2020 May 18

doi:10.1093/mnras/staa1373

Cross-correlating 21 cm and galaxy surveys: implications for cosmology and astrophysics

Hamsa Padmanabhan [1,2★] Alexandre Refregier[2] and Adam Amara[2,3]

[1] *Canadian Institute for Theoretical Astrophysics, 60 St. George St., Toronto, ON M5S 3H8, Canada*
[2] *Institute for Particle Physics and Astrophysics, ETH Zurich, Wolfgang-Pauli-Strasse 27, CH-8093 Zürich, Switzerland*
[3] *Institute of Cosmology & Gravitation, University of Portsmouth, Dennis Sciama Building, Burnaby Road, Portsmouth PO1 3FX, UK*

Accepted 2020 May 11. Received 2020 April 24; in original form 2019 September 24

ABSTRACT

We forecast astrophysical and cosmological parameter constraints from synergies between 21 cm intensity mapping and wide-field optical galaxy surveys (both spectroscopic and photometric) over $z \sim 0$–3. We focus on the following survey combinations in this work: (i) a CHIME-like and DESI-like survey in the Northern hemisphere, (ii) an LSST-like and SKA I MID-like survey, and (iii) a MeerKAT-like and DES-like survey in the Southern hemisphere. We work with the ΛCDM cosmological model having parameters $\{h, \Omega_m, n_s, \Omega_b, \sigma_8\}$, parameters $v_{c,0}$ and β representing the cut-off and slope of the H I–halo mass relation in the previously developed H I halo model framework, and a parameter Q that represents the scale dependence of the optical galaxy bias. Using a Fisher forecasting framework, we explore (i) the effects of the H I and galaxy astrophysical uncertainties on the cosmological parameter constraints, assuming priors from the present knowledge of the astrophysics, (ii) the improvements on astrophysical constraints over their current priors in the three configurations considered, and (iii) the tightening of the constraints on the parameters relative to the corresponding H I autocorrelation surveys alone.

Key words: cosmology: observations – cosmology: theory – radio lines: galaxies.

1 INTRODUCTION

Intensity mapping of redshifted emission lines (Bharadwaj, Nath & Sethi 2001; Loeb & Wyithe 2008) is a novel technique that has the potential to perform precision cosmology by detecting the integrated emission from sources across redshifts without resolving individual systems (e.g. Kovetz et al. 2019). Besides offering rich insights into the physics of star formation history and the processes governing galaxy evolution (e.g. Wyithe & Loeb 2008; Wolz et al. 2016), it has the ability to improve vastly upon the current measurements of cosmological parameters (e.g. Bull et al. 2015), as well as place competitive constraints on inflationary scenarios and physics beyond the standard model (e.g. Masui et al. 2010; Camera et al. 2013; Hall, Bonvin & Challinor 2013; Pourtsidou et al. 2016). The most well-studied example of line-intensity mapping involves that of the redshifted 21 cm emission of neutral hydrogen (hereafter, H I) which arises primarily in star-forming galaxies and the intergalactic medium at low to moderate redshifts.

Using line-intensity mapping techniques in synergy with other, more traditional and established tracers of large-scale structure is crucial to unlock the true potential of these surveys. It is known that (e.g. Seljak 2009; Camera et al. 2015; Fonseca et al. 2015; Fonseca, Maartens & Santos 2017) cross-correlations of several individual tracers of the cosmological structure often offer several significant advantages over individual surveys. The systematic survey-specific effects are mitigated to a large extent, the noise in the surveys is reduced, and the foregrounds and contaminants of individual surveys are, in most cases, uncorrelated and hence do not bias the cross-correlation measurement.[1] The cosmic variance can be mitigated in the measurement of some of the cosmological parameters (e.g. McDonald & Seljak 2009; Abramo & Leonard 2013).

To this end, cross-correlating 21 cm intensity mapping surveys with optical galaxies offers rich possibilities into exploiting the complementarity of both approaches. The first intensity mapping detection of the redshifted 21 cm emission at $z \sim 0.53$–1.12 with the Green Bank Telescope (GBT) was made in cross-correlation with the DEEP2 optical galaxy survey (Chang et al. 2013), and has been followed up since then resulting an updated cross-power spectrum using the WiggleZ survey at $z \sim 0.8$ (Masui et al. 2013)

[1] However, we note that the presence of foregrounds may greatly increase the variance, which is an important effect, and hence efficient foreground cleaning or avoidance techniques are still necessary in order to isolate the true signal.

★ E-mail: hamsa@cita.utoronto.ca

and an upper limit on the autopower spectrum (Switzer et al. 2013), which was used to place the first intensity mapping constraints on the product of the neutral hydrogen density and bias parameter. Similarly, the cross-power spectrum between 2dF galaxies in the Southern hemisphere and the Parkes H I intensity field at $z \sim 0$ has also been measured recently (Anderson et al. 2018), offering insights into the clustering of low-redshift H I systems.

The autocorrelation power spectrum signal of high-redshift 21 cm in emission has yet to be observed, although there are several experiments planned or in the final stages of commissioning to achieve this goal. These include (i) the Canadian Hydrogen Intensity Mapping Experiment (CHIME),[2] (ii) the Hydrogen Intensity and Real-time Analysis eXperiment (HIRAX),[3] (iii) the BAO In Neutral Gas Observations (BINGO; Battye et al. 2012), (iv) the TianLai experiment (Chen 2012) and the Five hundred metre Aperture Spherical Telescope (FAST; Smoot & Debono 2017), (v) the Meer-Karoo Array Telescope (MeerKAT; Jonas 2009), and (vi) the Square Kilometre Array (SKA) Phase I MID.[4]

The optical surveys of key interest for cross-correlations with the 21 cm surveys planned above include those with (i) the completed Dark Energy Survey (DES),[5] a photometric galaxy survey over $z \sim 0.5$–1.4, cataloging hundreds of millions of galaxies in the Southern hemisphere, (ii) the forthcoming Dark Energy Spectroscopic Instrument (DESI), a spectroscopic survey which will target a few tens of millions of galaxies in the northern sky over the redshift range $z \sim 0$–3, measuring cosmological parameters and the growth of structure through redshift space distortions, and (iii) future galaxy surveys conducted with the Large Synoptic Survey Telescope (LSST),[6] and the space-based *Euclid*[7] spectroscopic survey.

In Pourtsidou et al. (2016), synergies between a MeerKAT H I intensity mapping survey and photometric galaxies from the DES have been explored. Recent studies (Witzemann, Pourtsidou & Santos 2019b; Jalilvand et al. 2020) have illustrated the ability of H I intensity mapping (with SKA and HIRAX) in cross-correlation with photometric galaxy surveys (such as DES and LSST) to measure the gravitational lensing magnification. In Carucci, Villaescusa-Navarro & Viel (2017), the synergies between 21 cm SKA I MID and the Baryon Oscillation Spectroscopic Survey (BOSS)-like Ly α, surveys have been presented, which can constrain the bias of astrophysical systems. In Cosmic Visions 21 cm Collaboration (2018), various prospects for cross-correlating 21 cm intensity mapping and optical surveys have been explored, including with QSOs observed by the DESI survey. It has been shown (Chen et al. 2019) that combining a CMB Stage 4-like survey with 21 cm intensity mapping observations from an SKA I MID like survey cross-correlated with DESI quasars can enable precise measurements of the growth factor and test the predictions of general relativity on the largest scales. Witzemann et al. (2019a) explore how synergies between an SKA I MID like survey and a photometric LSST survey can mitigate the effects of cosmic variance, enabling measurements of the bias ratio at large scales up to $\ell \sim 3$, and Hall & Bonvin (2017) illustrate how peculiar velocity effects can be constrained using the dipole of the redshift space cross-correlation between 21 cm and optical surveys conducted with various experiments. In Ballardini, Matthewson & Maartens (2019), the constraints for local primordial non-Gaussianity has been studied with an SKA-like intensity mapping survey in cross-correlation with photometric galaxy surveys (Euclid and LSST) and CMB lensing.

In this paper, we build upon our previous forecasting analyses in Padmanabhan, Refregier & Amara (2019, hereafter Paper I) which focused on autocorrelation 21 cm power spectra and extend these to the case of measurement of the astrophysical and cosmological parameters using a combination of 21 cm and optical galaxy surveys. We use the uncertainties in the parameters coming from the combination of current measurements to set realistic priors on the H I astrophysics. We consider three sets of surveys in this work: (i) a CHIME-like survey overlapping with DESI in the Northern hemisphere, (ii) a MeerKAT-like survey overlapping with DES in the Southern hemisphere, and (iii) an SKAI MID survey overlapping with the LSST, again in the Southern hemisphere.

The paper is organized as follows. For modelling the H I distribution and density profile, we use the halo model framework introduced in Padmanabhan & Refregier (2017) and expanded upon in Padmanabhan, Refregier & Amara (2017, hereafter Paper II), which describes the best-fitting H I–halo mass relation and profile constrained by the currently available data. The bias and redshift distribution of the optical galaxies are modelled following the treatment for the particular survey under consideration. These frameworks are briefly described in Section 2. Using the cross-correlation power spectrum thus derived, we compute the relative errors on the astrophysical and cosmological parameters under consideration using a Fisher forecasting formalism for the three survey sets in Section 3. We comment on the comparison of these predictions to those from the corresponding 21 cm autocorrelation constraints and summarize our conclusions in Section 4.

2 FRAMEWORK FOR FISHER FORECASTS

We use the halo model for neutral hydrogen (see Paper II) and build upon our existing forecasts in Paper I, which had focused on the H I autocorrelation surveys alone. The halo model framework consists of a prescription assigning average H I mass to halo mass M at redshift z, given by

$$M_{\rm H\,I}(M,z) = \alpha f_{\rm H,c} M \left(\frac{M}{10^{11}h^{-1}{\rm M}_\odot}\right)^{\beta} \times \exp\left[-\left(\frac{v_{c0}}{v_c(M,z)}\right)^3\right] \quad (1)$$

In the above formula, the free parameters are given by: (i) α, the average H I fraction relative to cosmic $f_{\rm H,\,c}$, (ii) β, the logarithmic slope which represents the deviation from linearity of the H I–halo mass prescription, and (iii) v_{c0}, which denotes the minimum virial velocity below which haloes preferentially do not host H I.

To model the smaller scales in the H I power spectrum, we also need a prescription for the profile of the H I as a function of radius, halo mass, and redshift, which is found to be well modelled by an exponential function (Paper II, see also the observational results from, e.g. Bigiel & Blitz 2012):

$$\rho(r, M) = \rho_0 \exp(-r/r_{\rm s}) \quad (2)$$

with the scale radius $r_{\rm s}$ given by

$$r_{\rm s} = R_{\rm v}(M,z)/c_{\rm H\,I}(M,z) \quad (3)$$

with $R_{\rm v}$ being the halo virial radius and $c_{\rm H\,I}$ being the concentration parameter of the H I systems, which is analogous to the correspond-

[2] https://chime-experiment.ca/
[3] https://www.acru.ukzn.ac.za/hirax/
[4] http://www.ska.ac.za/
[5] https://www.darkenergysurvey.org/
[6] www.lsst.org
[7] www.euclid-ec.org

ing expression for dark matter:

$$c_{\rm H\,I}(M, z) = c_{\rm H\,I,0}\left(\frac{M}{10^{11}{\rm M}_\odot}\right)^{-0.109}\frac{4}{(1+z)^\gamma}. \quad (4)$$

The H I profile thus introduces two more free parameters through the concentration parameter and its evolution: (i) $c_{\rm H\,I,0}$ representing the overall normalization and γ which encodes the evolution of the function with redshift. In order to compute the nonlinear H I power spectrum, we need the Fourier transform of the profile function, given by

$$u_{\rm H\,I}(k|M) = \frac{4\pi}{M_{\rm H\,I}(M)}\int_0^{R_{\rm v}}\rho_{\rm H\,I}(r)\frac{\sin kr}{kr}r^2\,{\rm d}r \quad (5)$$

which allows us to write the power spectrum for H I intensity fluctuations as the sum of the 1- and 2-halo terms:

$$P_{\rm H\,I}(k, z) = P_{\rm 1h,H\,I} + P_{\rm 2h,H\,I} \quad (6)$$

with

$$P_{\rm 1h,H\,I}(k, z) = \frac{1}{\bar{\rho}^2_{\rm H\,I}}\int {\rm d}M\; n(M)\; M^2_{\rm H\,I}\;|u_{\rm H\,I}(k|M)|^2 \quad (7)$$

and

$$P_{\rm 2h,H\,I}(k, z) = P_{\rm lin}(k)\left[\frac{1}{\bar{\rho}_{\rm H\,I}}\int {\rm d}M\; n(M)\; M_{\rm H\,I}(M) \times\; b(M)\;|u_{\rm H\,I}(k|M)|\right]^2 \quad (8)$$

with $P_{\rm lin}(k)$ being the linear matter power spectrum.

For computing the power spectrum of the optical galaxies in the survey, we use the expression:

$$P_{\rm gal}(k, z) = P_{\rm dm}(k, z)\; b^2_{\rm gal}(k, z) \quad (9)$$

where $P_{\rm dm}$ is the dark matter power and the $b^2_{\rm gal}(k, z)$ denotes the galaxy–galaxy bias factor. This factor changes according to the survey and the type of galaxies under consideration. This (scale-dependent bias) is modelled following the parameters given by Amendola et al. (2017) which is based on the Q-formula of Cole et al. (2005):

$$b_{\rm gal} = b_{\rm gal,ls}b_0\left(\frac{1+Qk^2}{1+Ak}\right)^{1/2} \quad (10)$$

where the values $b_0 = 1.3$, $A = 1.7$, $Q = 4.6$ are assumed not to vary with redshift. The $b_{\rm gal,\,ls}$ term depends on the survey under consideration.

The angular power spectrum on the sky for H I is computed by using the standard result:

$$C_{\ell,{\rm H\,I}}(z, z') = \frac{2}{\pi}\int {\rm d}\tilde{z}\; W_{\rm H\,I}(\tilde{z})\int {\rm d}\tilde{z}'\; W'_{\rm H\,I}(\tilde{z}') \times\int k^2{\rm d}k\;\langle\delta_{\rm H\,I}(\mathbf{k}, z)\delta_{\rm H\,I}(\mathbf{k}', z')\rangle \times j_\ell(kR(\tilde{z}))j_\ell(kR(\tilde{z}')). \quad (11)$$

In the above expression, $\langle\delta_{\rm H\,I}(\mathbf{k}, z)\delta_{\rm H\,I}(\mathbf{k}', z')\rangle$ is the ensemble average of the H I density fluctuations at $(\mathbf{k}, z)$ and $(\mathbf{k}', z')$ respectively. This is, in general, not expressible purely in terms of the power spectrum of H I as defined above, $P_{\rm H\,I}(k, z)$ evaluated at either of $\{z, z'\}$ since the density field evolves with z. However, in many cases, one can approximate this as $P_{\rm H\,I}(k, z_{\rm m})$ where $z_{\rm m}$ is the mean redshift of the given bin. In what follows, we use z and $z_{\rm m}$ interchangeably.

In the above expression, the $W_{\rm H\,I}$, $W'_{\rm H\,I}$ are the H I window functions at the redshifts z and z', taken to be uniform across the redshift bin considered, and $R(z)$ is the comoving distance to redshift z. We use a top hat window function $W_{\rm H\,I}(z)$ with a width of $\Delta z = 0.5$.

For a generic galaxy survey, calculation of the angular power spectrum yields the expression

$$C_{\ell,{\rm gal}}(z, z') = \frac{2}{\pi}\int {\rm d}\tilde{z}\; W_{\rm g}(\tilde{z})\int {\rm d}\tilde{z}'\; W'_{\rm g}(\tilde{z}') \times\int k^2{\rm d}k\; P_{\rm gal}(k, z)j_\ell(kR(\tilde{z}))j_\ell(kR(\tilde{z}')). \quad (12)$$

The dark matter power spectrum for linear scales can alternatively be written as $P_{\rm dm}(k, z) = P_{\rm dm}(k, 0)D^2(z)$ where $D(z)$ is the growth factor for the dark matter perturbations whose power spectrum is normalized such that $D(0) = 1$. The window function for the galaxy survey, $W_{\rm g}$, can be different from that of the H I, and depends on the details of the selection function (usually denoted by $\phi(z)$) of each survey. Parametrized forms for $\phi(z)$ are available for different galaxy surveys and usually follow a standard functional form (Smail et al. 1995):

$$\phi(z) \propto z^\alpha\exp(-(z/z_0)^\beta) \quad (13)$$

where α, β, and z_0 are fitted from the galaxy counts data in different redshift bins. Once $\phi(z)$ is known, we derive the window function for the survey as

$$W_{\rm g}(z) = \phi(z)/\int_{z_{\rm min}}^{z_{\rm max}}\phi(z){\rm d}z \quad (14)$$

where $z_{\rm min}$ and $z_{\rm max}$ are the redshift edges of the survey. This ensures that the window function is normalized, i.e.

$$\int_{z_{\rm min}}^{z_{\rm max}} W_g(z){\rm d}z = 1. \quad (15)$$

The calculation of the angular power spectra above, both for H I and for galaxies, can be simplified on using the Limber approximation (Limber 1953) which is a good approximation in the large ℓ ($\ell > 50$) limit. The expression can be shown to reduce to

$$C_{\ell,{\rm H\,I/gal}} = \frac{1}{c}\int {\rm d}z\frac{W_{\rm H\,I/gal}(z)^2H(z)}{R(z)^2}P_{\rm H\,I,gal}[\ell/R(z), z]. \quad (16)$$

The cross-correlation signal is then calculated as

$$C_{\ell,\times} = \frac{1}{c}\int {\rm d}z\frac{W_{\rm H\,I}(z)W_{\rm gal}(z)H(z)}{R(z)^2}(P_{\rm H\,I}P_{\rm gal})^{1/2} \quad (17)$$

where the arguments of both power spectra ($P_{\rm H\,I}$ and $P_{\rm gal}$) are at $[\ell/R(z), z]$. Noise in the H I intensity mapping survey, for the MeerKAT-like and SKA I MID-like configurations, is calculated using the standard expression assuming the interferometer array to operate in the single-dish autocorrelation mode (e.g. Knox 1995; Ballardini & Maartens 2019):

$$N_{\ell,{\rm H\,I}} = \left(\frac{T_{\rm sys}}{\bar{T}(z)}\right)^2\left(\frac{\lambda_{\rm obs}}{D_{\rm dish}}\right)^2\left(\frac{1}{2N_{\rm dish}t_{\rm pix}\Delta\nu}\right)W^2_{\rm beam}(\ell). \quad (18)$$

In the above expression, $N_{\rm dish}$ denotes the number of interferometer dishes, each assumed to have the diameter $D_{\rm dish}$, and $\lambda_{\rm obs}$ is the observed wavelength. The $\bar{T}(z)$ is the mean brightness temperature at redshift z defined by

$$\bar{T}(z) \simeq 44\;\mu{\rm K}\left(\frac{\Omega_{\rm H\,I}(z)h}{2.45\times10^{-4}}\right)\frac{(1+z)^2}{E(z)}, \quad (19)$$

where $E(z) = H(z)/H_0$ is the normalized Hubble parameter at that redshift. The $T_{\rm sys}$ is the system temperature, calculated following

$T_{\rm sys} = T_{\rm inst} + 60\,{\rm K}(\nu/300\,{\rm MHz})^{-2.5}$ where $T_{\rm inst}$ is the instrument temperature and ν is the observing frequency. The quantity $W^2_{\rm beam}(\ell)$ denotes the beam window function due to the finite angular resolution of the instrument operating in single-dish mode (e.g. Pourtsidou et al. 2016), and is given by

$$W^2_{\rm beam}(\ell) = \exp\left[\frac{\ell(\ell+1)\theta_B^2}{8\ln 2}\right], \tag{20}$$

where $\theta_B \approx \lambda_{\rm obs}/D_{\rm dish}$ is the beam full width at half-maximum of a single dish.

The integration time per beam is $t_{\rm pix}$ and the $\Delta\nu$ denotes the frequency band channel width, which is connected to the tomographic redshift bin separation Δz. For the purposes of the noise calculation, we assume that $\Omega_{\rm HI}(z)h = 2.45 \times 10^{-4}$, independent of redshift.

For the CHIME-like experiment we consider, we use the full interferometric noise expression, which is given by

$$N_{\ell,\rm CHIME} = \frac{4\pi f_{\rm sky}}{{\rm FoV}n_{\rm base}(u)n_{\rm pol}N_{\rm beam}t_{\rm tot}\Delta\nu}\left(\frac{T_{\rm sys}}{\bar{T}}\right)^2\left(\frac{\lambda^2_{\rm obs}}{A_{\rm eff}}\right)^2. \tag{21}$$

In the above equation, $N_{\rm beam}$ is the number of independent beams, and for CHIME, $N_{\rm beam} = Nf \times N_{\rm cyl}$ where $N_{\rm f} = 256$ is the number of feeds, and $N_{\rm cyl} = 4$ is the number of cylinders. Each is assumed to have the effective area $A_{\rm eff} = \eta L_{\rm cyl}W_{\rm cyl}/N_f$, where $\eta = 0.7$, $W_{\rm cyl} = 20\,{\rm m}$ is the width of each cylinder, and $L_{\rm cyl} = 100\,{\rm m}$ is its length. The total integration time, denoted by $t_{\rm tot}$ is taken to be 1 yr for the CHIME-like survey considered here. The $n_{\rm pol}$ is the number of polarization channels (taken to be 2). The baseline number density is $n_{\rm base}(u)$, expressible in terms of the multipole ℓ via $u = \ell/(2\pi)$. This quantity is approximated as independent of u up to a maximum baseline length $u_{\rm max}$, viz. $n_{\rm base}(u) = N^2_{\rm beam}/(2\pi u^2_{\rm max})$. The $u_{\rm max}$ denotes the longest baseline $d_{\rm max}$ measured in wavelength units, $u_{\rm max} = d_{\rm max}/\lambda_{\rm obs}$, with $d_{\rm max} = 269\,{\rm m}$ for CHIME (Obuljen et al. 2018). The field of view for the CHIME interferometer is approximated as FoV $\approx \pi/2 \times \lambda/W_{\rm cyl}$ (Newburgh et al. 2014) for this configuration.

The noise for the galaxy survey is taken to be the (Poisson) shot noise, calculated as $N_{\ell,\rm gal} = n^{-1}_{\rm gal,bin}(z)$ where $n_{\rm gal,\,bin}(z)$ is the number density of galaxies per steradian in the bin centred at redshift z. Given the selection function of the galaxies, $\phi(z)$ defined in equation (13), this quantity is computed as

$$n_{\rm gal,bin}(z) = \int_{z-\Delta z/2}^{z+\Delta z/2}\phi(z'){\rm d}z'. \tag{22}$$

Finally, the variance of the forecasted angular power spectrum is calculated as

$$(\Delta C_{\ell,\times})^2 = \frac{1}{(2\ell+1)\Delta\ell f_{\rm sky,\times}}\left[\left(C_{\ell,\rm HI} + N_{\ell,\rm HI}\right)\right.$$
$$\left.\times\left(C_{\ell,\rm gal} + N_{\ell,\rm gal}\right) + C^2_{\ell,\times}\right]. \tag{23}$$

In the above expression, the quantity $f_{\rm sky,\,\times}$ denotes the sky coverage of the overlap between the surveys. For simplicity, an optimistic complete overlap is assumed, and hence throughout this work, $f_{\rm sky,\,\times}$ denotes the smaller of the two sky coverages of the galaxy and H I redshift survey, respectively. We use 15 ℓ-bins between $\ell = 1$ and $\ell = 1000$, logarithmically spaced with $\Delta\log_{10}\ell = 0.2$.

We use a Fisher forecasting formalism to place constraints on the cosmological and astrophysical parameters, given the experimental configuration under consideration. The Fisher matrix is computed as follows:

$$F_{ij} = \sum_\ell \frac{1}{(\Delta C_{\ell,\times})^2}\frac{\partial C_{\ell,\times}}{\partial p_i}\frac{\partial C_{\ell,\times}}{\partial p_j} \tag{24}$$

where the sum is over the range of ℓ's probed, and the p_i's denote the individual parameters.

The following parameters are used for the computation of the cross-power spectrum of H I and galaxy surveys:

(i) The H I-based astrophysical parameters include $v_{c,0}$, α, and β used in the $M_{\rm HI}(M)$ relation, and the two parameters $c_{\rm HI,0}$ and γ for the H I profile,

(ii) the galaxy astrophysics contains the three parameters b_0, $b_{\rm ls}$, Q and A used in the large-scale and the scale-dependent part of the bias respectively, and

(iii) the cosmological parameters are the Hubble parameter h, the baryon density $\Omega_{\rm b}$, the spectral index $n_{\rm s}$, the power spectrum normalization parameter σ_8, and the cosmological matter density, $\Omega_{\rm m}$.

Of the H I astrophysical parameters, only two, viz. the cut-off and the slope of the H I–halo mass relation, i.e. $v_{c,0}$ and β are relevant for forecasting with H I intensity mapping surveys (see Paper I for details). While we use all the galaxy parameters to model the bias for various surveys, we vary only the parameter Q encoding the scale dependence of the bias. Throughout the analysis, the cosmology adopted is flat, i.e. $\Omega_\Lambda = 1 - \Omega_{\rm m}$. The fiducial values of the cosmological and astrophysical parameters are listed in Table 1.

Table 1. Fiducial values of the astrophysical and cosmological parameters considered. Astrophysical parameters come from the best-fitting values of the halo model for neutral hydrogen (Paper II), and that of the galaxy Q parameter from the 'blue5' galaxy sample in Cresswell & Percival (2009). The cosmological parameters are in good agreement with most available observations, including the latest Planck results (Planck Collaboration 2014).

Astrophysical		Cosmological	
$\log(v_{c,0}/{\rm km\,s^{-1}})$	1.56	h	0.71
β	−0.58	$\Omega_{\rm m}$	0.28
Q	4.6	$\Omega_{\rm b}$	0.0462
		σ_8	0.81
		ns	0.963

For calculating the standard deviations of the various cosmological and astrophysical parameters, we use a procedure similar to Paper I: we consider equal sized redshift bins of width $\Delta z \approx 0.5$ each, spanning the desired cross-correlation range in redshift, and evaluate the Fisher matrices F_{ij} given by equation (24) at the mid-points of each of the bins. The cumulative Fisher matrix for the $z-$range is derived from tomographic addition of the bins: $F_{ij,\rm cumul} = \sum_{\Delta z\in z} F_{ij}$, which is the sum of the individual Fisher matrices, F_{ij} in each of the $z-$bins of width Δz contained between 0 and z. From the cumulative Fisher matrix, the standard errors in the parameters are computed for various cases. We ignore the effects of cross-correlations between individual bins and those between galaxies and H I in adjacent bins.

3 EXPERIMENT COMBINATIONS

For each galaxy survey, the specifications include the large-scale galaxy bias, $b_{\rm gal,\,ls}$, the selection function $\phi(z)$, and the total number

Table 2. Various experimental configurations considered in this work.

Configuration	Galaxy $n_{\rm gal}$ (arcmin^{-2})	$b_{\rm ls,\,gal}$	H I $T_{\rm inst}$ (K)	H I $N_{\rm dish}$	H I $D_{\rm dish}$ (m)	Cross-correlation $f_{\rm sky,\,\times}$	$z_{\rm bins}$
CHIME-DESI	0.33	$0.84/D(z)$	50	1280	20	0.44	[0.8, 1.2, 1.6]
MeerKAT-DES	8	$(1.07-0.35z)^{-1}$	29	64	13.5	0.12	[0.5, 1.0, 1.4]
SKA I MID-LSST	26	$1.46(1+0.84z)$	28	190	15	0.48	[0.082, 0.58, 1., 1.5, 2., 2.3, 3.06]

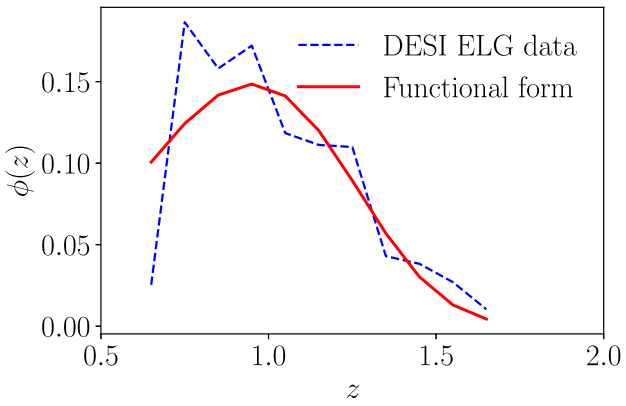

Figure 1. Redshift selection function constructed from the forecasted number counts for DESI ELG galaxies in DESI Collaboration (2016), along with its fitted functional form represented by equation (25).

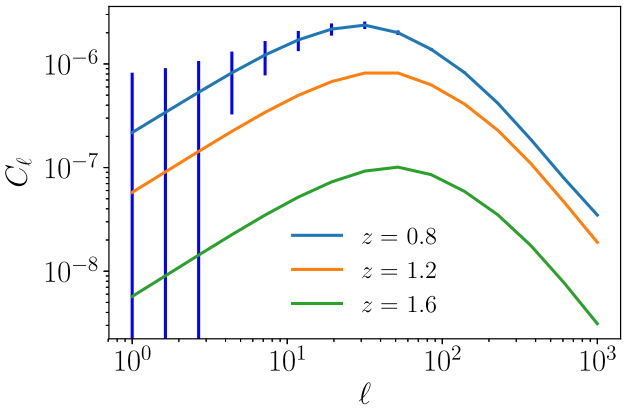

Figure 2. Cross-correlation power spectra for a CHIME-DESI like survey, at the three redshifts of interest. Error bars indicate the expected standard deviation of the angular power spectrum (equation 23) at the lowest redshift ($z \sim 0.8$).

density of galaxies, $n_{\rm gal}$. These as well as the survey properties of the H I surveys are listed together in Table 2.

3.1 CHIME and DESI

The redshift coverage of the cross-correlation is $0.8 < z < 1.8$. The CHIME autocorrelation survey runs over $z \sim 0.8$–2.5. The DESI sample is assumed to correspond to the Emission Line Galaxy (ELG) survey,[8] with the bias factor $b_{\rm gal,\,ls} = 0.84/D(z)$ where $D(z)$ is the growth factor. The selection function for DESI is constructed by numerically fitting to the number counts in the ELG forecasts over $z \sim 0.6$–1.8, table 2 of DESI Collaboration (2016). It is found that this selection function can be modelled as

$$\phi(z) \propto (z/z*)^2 \exp(-(z/z_0)^\beta), \tag{25}$$

where $z* = 1.96$, $z_0 = 1.14$, and $\beta = 4.36$. This selection function, as well as the raw number counts forecasted for DESI ELG galaxies, is plotted in Fig. 1. The surface number density of galaxies is $n_{\rm gal} \approx 0.33$ arcmin^{-2} (corresponding to roughly 1200 galaxies deg^{-2}), which is consistent with the estimates for the numbers of ELG targets in DESI Collaboration (2016).

The observing time $t_{\rm pix}$ is assumed to be 1 h (per pixel). The sky coverages for the individual surveys are taken as $f_{\rm sky}$ (CHIME) = 0.61 (corresponding to 25 000 deg^2) and $f_{\rm sky}$ (DESI) = 0.44 (corresponding to 18000 deg^2) and the DESI value is assumed for $f_{\rm sky,\,\times}$. We consider equal-sized redshift bins of width $\Delta z = 0.5$ each.

Plotted in Fig. 2 are the cross-correlation angular power spectra (computed following equation 17) for the CHIME-DESI like configuration at three mean redshifts 0.8, 1.2, and 1.6. At the lowest redshift, the error bars indicating the expected standard deviation on the power spectrum (from equation 23) are also plotted.

In Fig. 3 are plotted the cumulative fractional errors (combining all the redshifts under construction) on the forecasted cosmological and astrophysical (both H I and galaxy) parameters in the following cases: (a) with fixed cosmology, i.e. without marginalization over the cosmological parameters, (b) with fixed astrophysics, and (c) marginalizing over the galaxy and H I astrophysics, assuming a prior on the astrophysical parameters coming from the current knowledge of the H I and galaxy data. The extent of these astrophysical priors is plotted in violet. The H I parameters are assumed to have the best-fitting standard deviation values constrained by the presently available data (see table 3 of Padmanabhan et al. 2017).The galaxy parameter Q is taken to have a standard deviation of 1.78, following the discussion for the 'blue5' galaxy sample in Cresswell & Percival (2009).

The left-hand panel of Fig. 3 shows that the constraints in the CHIME-DESI cross-correlation case improve on the corresponding autocorrelation constraints using a CHIME-like configuration alone, by factors of about 1.1–2 depending on the cosmological parameter under consideration (comparing to fig. 7 of Paper I). It is notable that this improvement occurs even though the redshift coverage of the cross-correlation is only about half that of the autocorrelation survey, and illustrates the extent to which adding the galaxy survey information helps improve the cosmological constraints.

For all the three astrophysical parameters, there is a marked improvement on the current knowledge of the astrophysics from the cross-correlation information, as represented by the relative magnitudes of the violet and cyan/green bars. The constraints improve by factors of 3.5, 3.1, and 3.3 respectively compared to their current priors.

[8]This is the largest sample of galaxies for which DESI will obtain spectroscopic redshifts over $z \sim 0.6$–1.8.

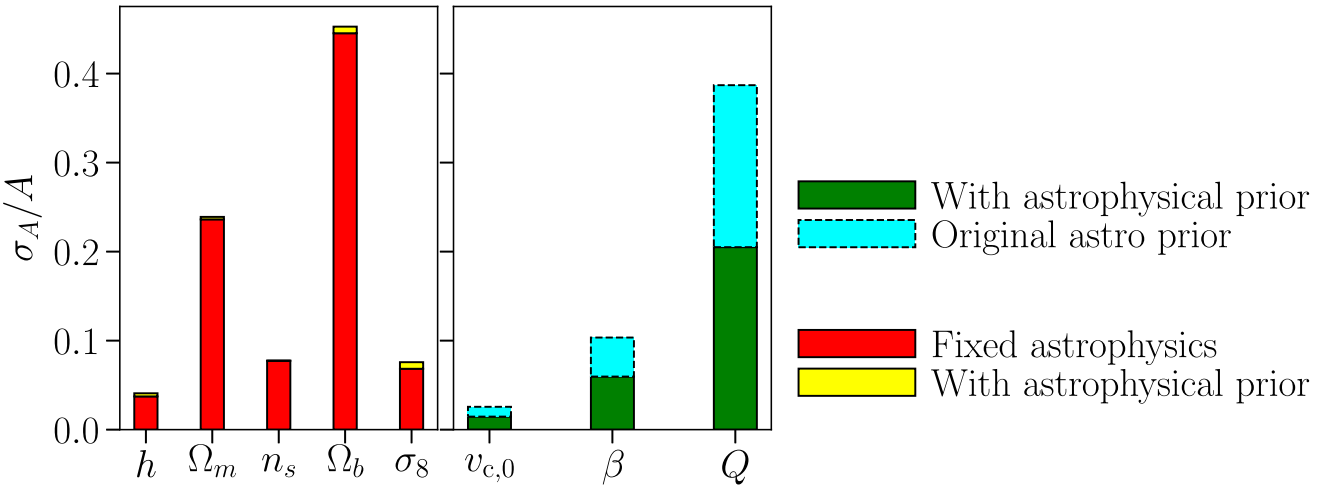

Figure 3. Cross-correlation forecasts on astrophysics and cosmology for a CHIME-DESI like survey. Fractional errors, σ_A/A are plotted with $A = \{h, \Omega_m, n_s, \Omega_b, \sigma_8, v_{c,0}, \beta, Q\}$, using information from all the redshift bins available over the combined data set. The left-hand panel shows the constraints on the cosmological parameters (i) without marginalizing over astrophysics and (ii) marginalizing over astrophysics but including a prior based on the current knowledge of the astrophysical parameters. The right-hand panel plots the constraints on the astrophysical parameters for the case of marginalizing over cosmology but adding the astrophysical prior. The extent of the astrophysical prior assumed is plotted as the cyan band for each case in the right-hand panel.

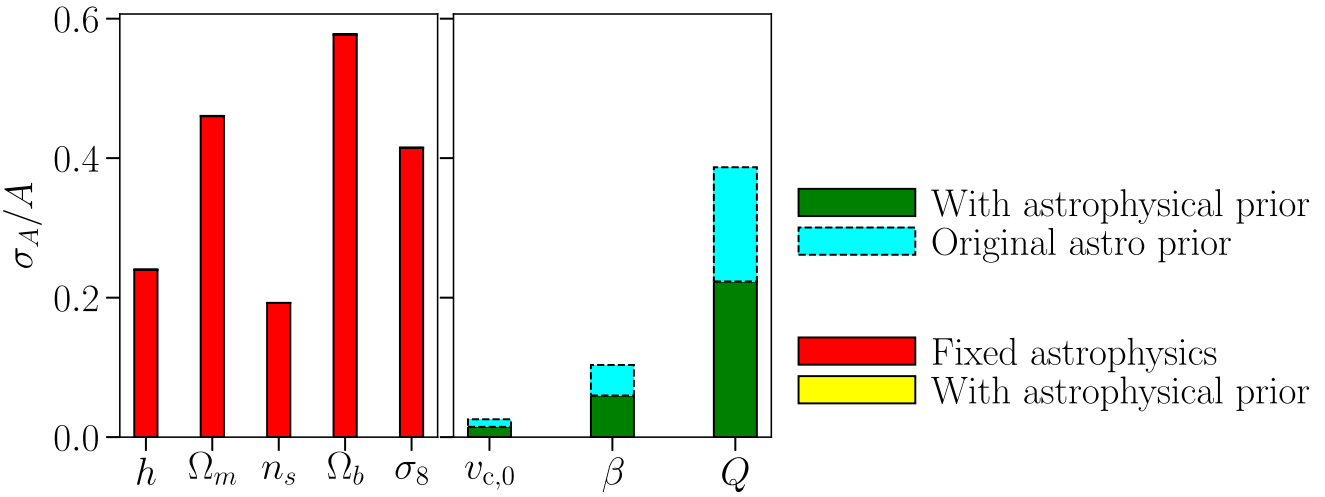

Figure 4. Same as Fig. 3, for a MeerKAT-DES like survey.

3.2 MeerKAT and DES

Pourtsidou et al. (2016) discussed the potential for forecasting lensing convergence parameters with a MeerKAT-DES survey in the Southern hemisphere.[9] Here, we explore how such a cross-correlation survey could potentially constrain the cosmological and astrophysical (both galaxy bias and H I) parameters as in the previous case.

The redshift coverage of the survey is taken to broadly cover $z = 0.2$ to $z = 1.4$. (Both DES and MeerKAT cover a similar redshift range, so the redshift overlap is stronger between these two surveys.) The sky coverage is assumed to be all of the DES survey, 5000 deg^2, thus assuming complete overlap. The galaxy bias for the DES galaxies is given by the fitting formula (Chang et al. 2016; Pujol et al. 2016): $b^{-1}_{\rm gal,ls} = 1.07 - 0.35z$. The redshift selection function for the DES galaxies is taken to have the form (e.g. Crocce, Cabré & Gaztañaga 2011):

$$\phi(z) \propto \left(\frac{z}{0.5}\right)^2 \exp\left(-\left(\frac{z}{0.5}\right)^{1.5}\right). \quad (26)$$

The surface number density of the DES galaxies under consideration is $n_{\rm gal} = 8$ arcmin^{-2}, consistent with the estimates in Becker et al. (2016).

The fractional errors on the parameters considered are plotted in Fig. 4. Errors in the 'fixed astrophysics case' remain essentially unchanged from those with the astrophysical prior. The constraints on the cosmological parameters are of the same order of magnitude as those from the MeerKAT autocorrelation survey. The astrophysical constraints improve over the current knowledge of these parameters as seen by the relative magnitudes of the cyan and the green bars, by factors of about 1.5-2 for $v_{c,0}$, β, and Q respectively.

[9]The MeerKLASS (MeerKAT Large Area Synoptic Survey; Santos et al. 2017) proposes to investigate galaxy evolution and cosmology using a 4000 deg^2 overlap with the Dark Energy Survey (DES).

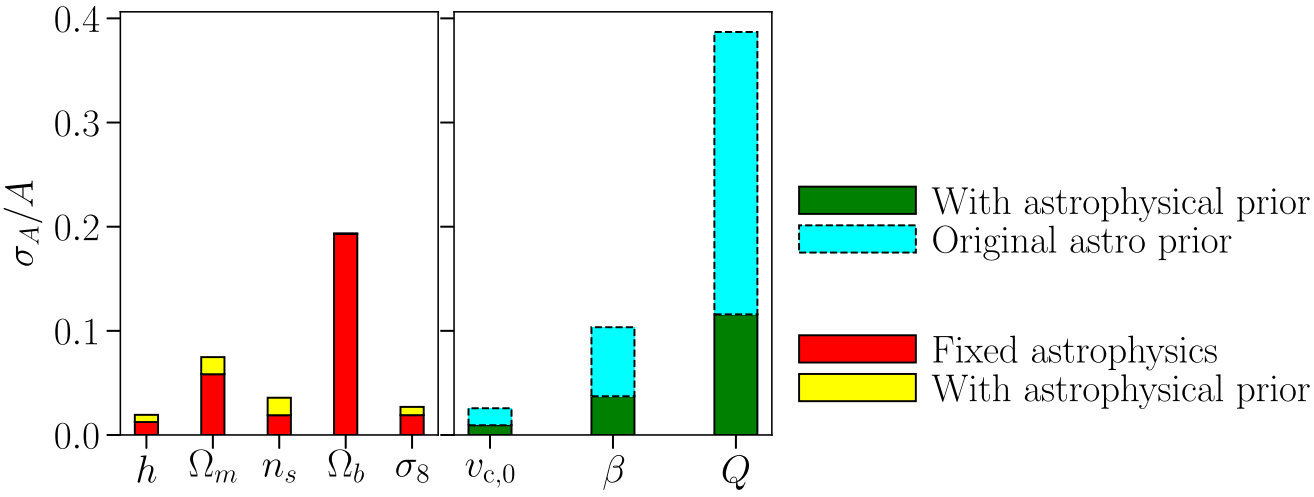

Figure 5. Same as Fig. 3, for an LSST-SKA like survey.

3.3 SKA I MID and LSST

The Large Synoptic Survey Telescope (LSST) survey parameters are taken to be (LSST Science Collaboration 2009), see also Chang et al. (2013) and Ferraro & Hill (2018): (i) the galaxy surface number density $n = 26$ arcmin^{-2} and (ii) large-scale bias $b_{\rm gal,\,ls} = 1.46(1 + 0.84z)$. The redshift coverage is from $z \sim 0$–3 which spans both the SKAI-MID (B1 and B2) bands. The redshift selection function of the survey is taken to be (Chang et al. 2013):

$$\phi(z) \propto z^{1.28} \exp\left(-\frac{z}{0.41}\right)^{0.97}. \tag{27}$$

The sky coverage of LSST is assumed to be 20000 deg^2 and that of the SKA-I is 25000 deg^2, and hence the LSST coverage is used for calculating $f_{\rm sky,\,\times}$ (assuming complete overlap).

This configuration leads to the tightest constraints on all the cosmological and astrophysical parameters as shown in Fig. 5, with all relative errors being about a few per cent. It also leads to a substantial improvement in the astrophysical constraints as compared with those from the present data.

The relative errors on the cosmological parameters reach values down to ∼0.01 with this configuration. Constraints on h, σ_8 and n_s with the astrophysical prior improve by factors of a few to ten, compared to the corresponding values from the SKA I - MID like autocorrelation survey alone (shown in Paper I), while those on $\Omega_{\rm m}$ and $\Omega_{\rm b}$ improve by factors 2–5. Further, the astrophysical parameters improve over their current priors by factors of 2.7, 2.8, and 3.3 for $v_{c,\,0}$, β, and Q, respectively.

4 CONCLUSIONS

In this paper, we have explored combining upcoming H I intensity mapping surveys with wide-field galaxy optical surveys to improve available constraints on astrophysical and cosmological parameters over $z \sim 0$–3 in the post-reionization universe. Using the ΛCDM cosmological parametrization, a halo model framework for H I driven by currently available data, and available optical galaxy parametrizations, we have studied the extent to which these constraints improve over their current uncertainties due to cross-correlation measurements. We also note the improvement in the constraints compared to those from the corresponding H I autocorrelation surveys alone.

For all three survey cases considered (a CHIME-DESI-like survey in the Northern hemisphere, and a MeerKAT-DES-like survey and an LSST-SKA-like survey in the Southern hemisphere), we find that the cross-correlation leads to improvements in measurement of both astrophysical and cosmological parameters, though the extent of improvement depends on the parameter under consideration. The significant benefit of cross-correlation (particularly in the MeerKAT-DES-like and CHIME-DESI-like configurations) lies in the improvement of astrophysical constraints. The halo model framework allows us to place realistic priors on the H I astrophysics from the currently available data. With the LSST-SKA combination, all the parameter constraints (both astrophysical and cosmological) reach levels below about 20 per cent, even without the assumption of cosmological priors.

The astrophysical forecasts for the H I and galaxy parameters improve substantially (by factors of a few) over their current priors, with the help of the cross-correlation measurements. This holds even in the presence of the additional galaxy parameter Q, which is seen to have comparable constraints though its prior knowledge is assumed to be more uncertain. The cosmological forecasts improve by factors of about a few (depending on the configuration) over those from the corresponding autocorrelation surveys alone.

We note that the foregrounds, which may be the limiting systematic, are excluded from the noise calculation in the present study. However, in the case of cross-correlation measurements, the foregrounds for the two individual probes are expected to be significantly uncorrelated and thus lead to negligible effects (as shown for the case of non-smooth foregrounds in 21 cm cross-correlations with LBG surveys in, e.g. Villaescusa-Navarro et al. 2015). Recent studies (Breysse, Anderson & Berger 2019; Cunnington et al. 2019; Modi et al. 2019) describe ways in which the signal, in the presence of foregrounds, may be reconstructed from 21 cm intensity mapping data cross-correlated with other tracers, such as the CMB or optical (both spectroscopic and photometric) galaxy surveys. A couple of caveats in this respect, however, are worth mentioning.

(i) First, we know that 21 cm experiments in autocorrelation suffer from bright foregrounds, which must be removed effectively, leading to a loss of low-k modes (this effect is particularly prominent for the low-k modes in the radial direction, which correspond to the largest scales). Hence, these Fourier modes are likely to be lost

from the survey information, even if systematic biases caused by foregrounds can be disregarded.

(ii) We have not explicitly modelled the effects of the galaxy photo-z errors in the present analysis. Since fairly broad redshift bins are used (with $\Delta z \sim 0.5$), the effect of these errors may be largely mitigated for the case of the galaxy–galaxy autocorrelation. However, if foreground filtering results in the removal of radial modes in the 21 cm surveys up to some maximum (as described in the previous point), then there may be little overlap between the 21 cm radial modes and the galaxy radial modes that remain for the cross-correlation. This effect may need careful treatment when foreground cleaning or avoidance is being considered.

Just as in the previous study with autocorrelation data alone (Paper II), we see that the overlap in redshift coverage is extremely important in tightening forecasts (due to more information coming from the addition of independent tomographic bins). Also, choosing similar sky area overlap between the H I and galaxy surveys (presently assumed to have complete overlap) would lead to better constraints on the parameters. Extending these approaches towards intensity mapping with other emission lines (CO, C II) would enable us to potentially form a comprehensive picture of galaxy evolution at the scales of the ISM. Ultimately, combining both auto- and cross-correlation forecasts, possibly with cosmological priors from present and future CMB experiments, would provide the tightest possible constraints exploiting the synergy of CMB, H I, and galaxy surveys. This would be a powerful tool to explore more parameters in cosmological models such as e.g. testing modifications to general relativity at the largest scales (e.g. Hall et al. 2013) with future wide-field surveys.

ACKNOWLEDGEMENTS

We thank Stefano Camera, Ue-Li Pen, and Renée Hložek for useful discussions, and the anonymous referee for a detailed and helpful report that improved the content and quality of the presentation. HP's research was supported by the Tomalla Foundation. AA is supported by the Royal Society Wolfson Fellowship.

REFERENCES

Abramo L. R., Leonard K. E., 2013, MNRAS, 432, 318
Amendola L., Menegoni E., Di Porto C., Corsi M., Branchini E., 2017, Phys. Rev. D, 95, 023505
Anderson C. J. et al., 2018, MNRAS, 476, 3382
Ballardini M., Maartens R., 2019, MNRAS, 485, 1339
Ballardini M., Matthewson W. L., Maartens R., 2019, MNRAS, 489, 1950
Battye R. A. et al., 2012, Proc. Moriond Cosmology, preprint (arXiv:1209.1041)
Becker M. R. et al., 2016, Phys. Rev. D, 94, 022002
Bharadwaj S., Nath B. B., Sethi S. K., 2001, J. Astrophys. Astron., 22, 21
Bigiel F., Blitz L., 2012, ApJ, 756, 183
Breysse P. C., Anderson C. J., Berger P., 2019, Phys. Rev. Lett., 123, 231105
Bull P., Ferreira P. G., Patel P., Santos M. G., 2015, ApJ, 803, 21
Camera S., Santos M. G., Ferreira P. G., Ferramacho L., 2013, Phys. Rev. Lett., 111, 171302
Camera S. et al., 2015, in Bourke T. L. , et al., eds, Proc. Sci. Vol. 215: Advancing Astrophysics with the Square Kilometre Array (AASKA14). SISSA, Trieste, PoS(AASKA14)025,
Carucci I. P., Villaescusa-Navarro F., Viel M., 2017, J. Cosmol. Astropart. Phys., 2017, 001
Chang C. et al., 2013, MNRAS, 434, 2121
Chang C. et al., 2016, MNRAS, 459, 3203
Chen S.-F., Castorina E., White M., Slosar A., 2019, J. Cosmol. Astropart. Phys., 2019, 23
Chen X., 2012, Int. J. Mod. Phys. Conf. Ser., 12, 256
Cole S. et al., 2005, MNRAS, 362, 505
Cosmic Visions 21 cm Collaboration, 2018, preprint (arXiv:1810.09572)
Cresswell J. G., Percival W. J., 2009, MNRAS, 392, 682
Crocce M., Cabré A., Gaztañaga E., 2011, MNRAS, 414, 329
Cunnington S., Wolz L., Pourtsidou A., Bacon D., 2019, MNRAS, 488, 5452
DESI Collaboration, 2016, preprint (arXiv:1611.00036)
Ferraro S., Hill J. C., 2018, Phys. Rev. D, 97, 023512
Fonseca J., Camera S., Santos M. G., Maartens R., 2015, ApJ, 812, L22
Fonseca J., Maartens R., Santos M. G., 2017, MNRAS, 466, 2780
Hall A., Bonvin C., 2017, Phys. Rev. D, 95, 043530
Hall A., Bonvin C., Challinor A., 2013, Phys. Rev. D, 87, 064026
Jalilvand M., Majerotto E., Bonvin C., Lacasa F., Kunz M., Naidoo W., Moodley K., 2020, Phys. Rev. Lett., 124, 031101
Jonas J. L., 2009, IEEE Proc., 97, 1522
Knox L., 1995, Phys. Rev. D, 52, 4307
Kovetz E. D. et al., 2019, BAAS, 51, 101
Limber D. N., 1953, ApJ, 117, 134
Loeb A., Wyithe J. S. B., 2008, Phys. Rev. Lett., 100, 161301
LSST Science Collaboration, 2009, preprint (arXiv:0912.0201)
McDonald P., Seljak U., 2009, J. Cosmol. Astropart. Phys., 2009, 007
Masui K. W., Schmidt F., Pen U.-L., McDonald P., 2010, Phys. Rev. D, 81, 062001
Masui K. W. et al., 2013, ApJ, 763, L20
Modi C., White M., Slosar A., Castorina E., 2019, J. Cosmol. Astropart. Phys., 2019, 023
Newburgh L. B. et al., 2014, Proc. SPIE Conf. Ser. Vol. 9145, Calibrating CHIME: a New Radio Interferometer to Probe Dark Energy. SPIE, Bellingham, p. 91454V
Obuljen A., Castorina E., Villaescusa-Navarro F., Viel M., 2018, J. Cosmol. Astropart. Phys., 2018, 004
Padmanabhan H., Refregier A., 2017, MNRAS, 464, 4008
Padmanabhan H., Refregier A., Amara A., 2017, MNRAS, 469, 2323 (Paper II)
Padmanabhan H., Refregier A., Amara A., 2019, MNRAS, 485, 4060 (Paper I)
Planck Collaboration, 2014, A&A, 571, A16
Pourtsidou A., Bacon D., Crittenden R., Metcalf R. B., 2016, MNRAS, 459, 863
Pujol A. et al., 2016, MNRAS, 462, 35
Santos M. G. et al., 2017, Proc. Sci., MeerKAT Science: On the Pathway to the SKA, Stellenbosch, preprint (arXiv:1709.06099)
Seljak U., 2009, Phys. Rev. Lett., 102, 021302
Smail I., Hogg D. W., Yan L., Cohen J. G., 1995, ApJ, 449, L105
Smoot G. F., Debono I., 2017, A&A, 597, A136
Switzer E. R. et al., 2013, MNRAS, 434, L46
Villaescusa-Navarro F., Viel M., Alonso D., Datta K. K., Bull P., Santos M. G., 2015, J. Cosmol. Astropart. Phys., 2015, 034
Witzemann A., Alonso D., Fonseca J., Santos M. G., 2019a, MNRAS, 485, 5519
Witzemann A., Pourtsidou A., Santos M. G., 2019b, preprint (arXiv:1907.00755)
Wolz L., Tonini C., Blake C., Wyithe J. S. B., 2016, MNRAS, 458, 3399
Wyithe J. S. B., Loeb A., 2008, MNRAS, 383, 606

This paper has been typeset from a TEX/LATEX file prepared by the author.